Electronic Supplementary Material (ESI) for Soft Matter.

Supplementary Figure 1

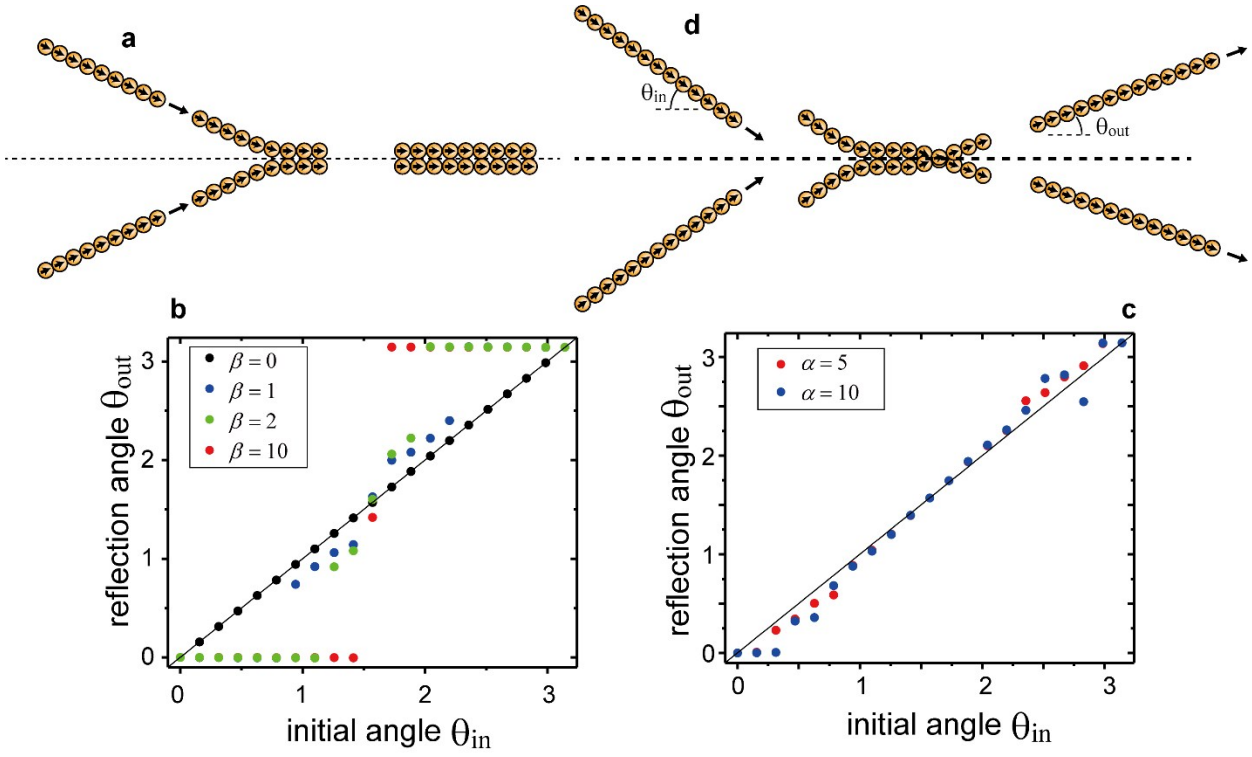

Supplementary Fig. 1: Collisions of two filaments in our model. (a,d) Schematic images of filament conformation during the collision for the steric (a) and alignment (d) interactions. (b,c) Reflection angles as a function of initial angles of the collision to characterize the degree of alignment ability. The steric interactions (b) and the alignment interactions (c) were used. The solid lines indicate that the reflection angles are unchanged from the initial angles during the collisions. Deviation from the solid line implies an inelastic collision with alignment if the reflection angles are below the line for initial angles less than $\pi/2$, and if they are above the line for initial angles larger than $\pi/2$. The opposite case indicates inhibition of alignment. Both interactions show alignment. Deviation for the steric interactions is larger, and this demonstrates the steric interactions have stronger alignment ability.

Supplementary Figure 2 (caption next page)

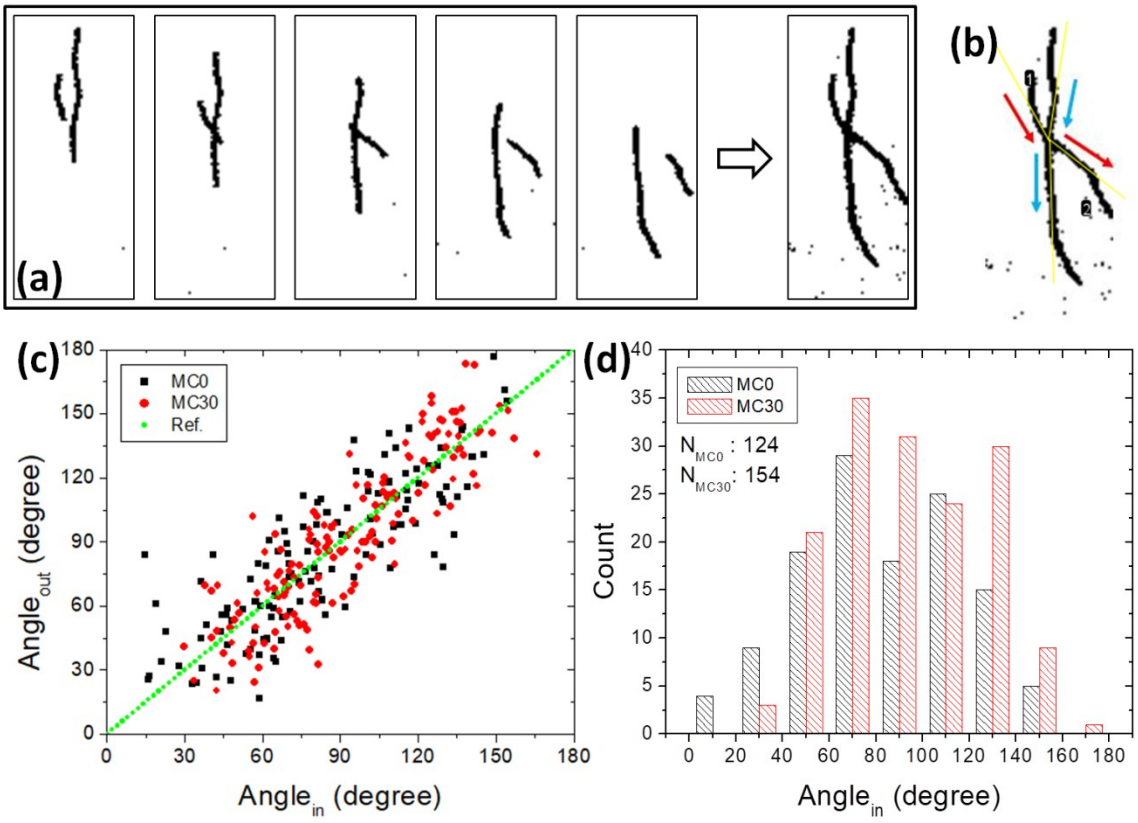

Supplementary Fig. 2: Analysis of MT crossing events. (a) Fluorescence images (binary format) of two gliding MTs crossing each other with time. The five panels are stacked up in the far right panel (right of the arrow) generating a trace of the gliding MTs. (b) Incident angle ((1), $Angle_{in}$) and outgoing angle ((2), $Angle_{out}$) denoted in the trace with yellow lines. Color-coded arrows follow each of the two MTs. (c) Scatter plot of $Angle_{in}$ versus $Angle_{out}$ for two different cases, with (MC30) and without (MC0) methyl cellulose. The reference line indicates $Angle_{in}$ /$Angle_{out}$ =1. (d) Incident angle histogram of MT crossing events. Total events: 124 for MC0 (three independent assays, four different areas for each assay) and 154 for MC30 (three independent assays, four different areas for each assay).

Supplementary Figure 3

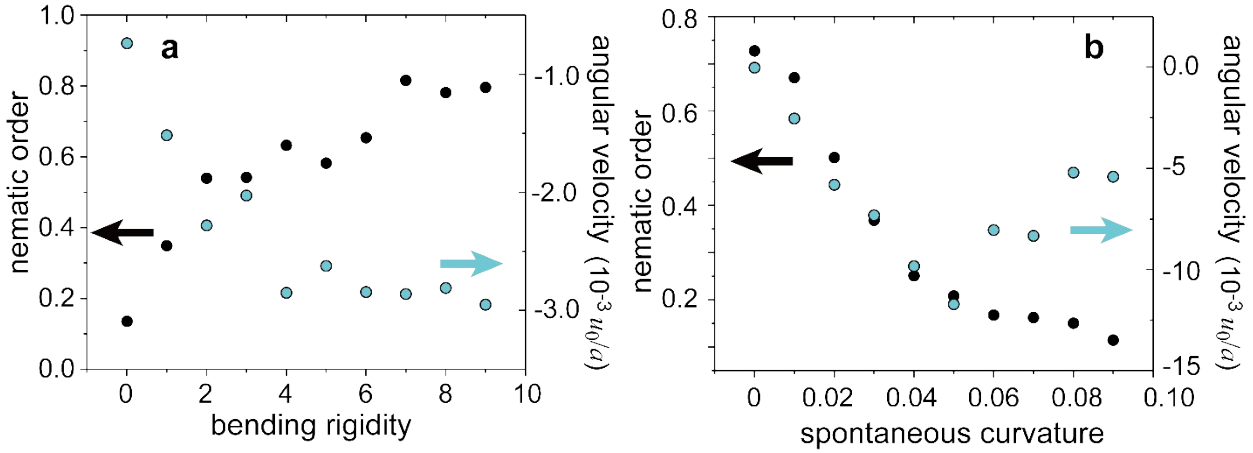

Supplementary Fig. 3: The nematic order parameter (black circles) and the angular velocity (light blue circles) dependence on bending rigidity (a) with $\alpha = 5, \beta = 0$ and $\theta_0 = 0.01$ and spontaneous curvature (b) with $\alpha = 5, \beta = 0$ and $\kappa = 5$.

Supplementary Figure 4

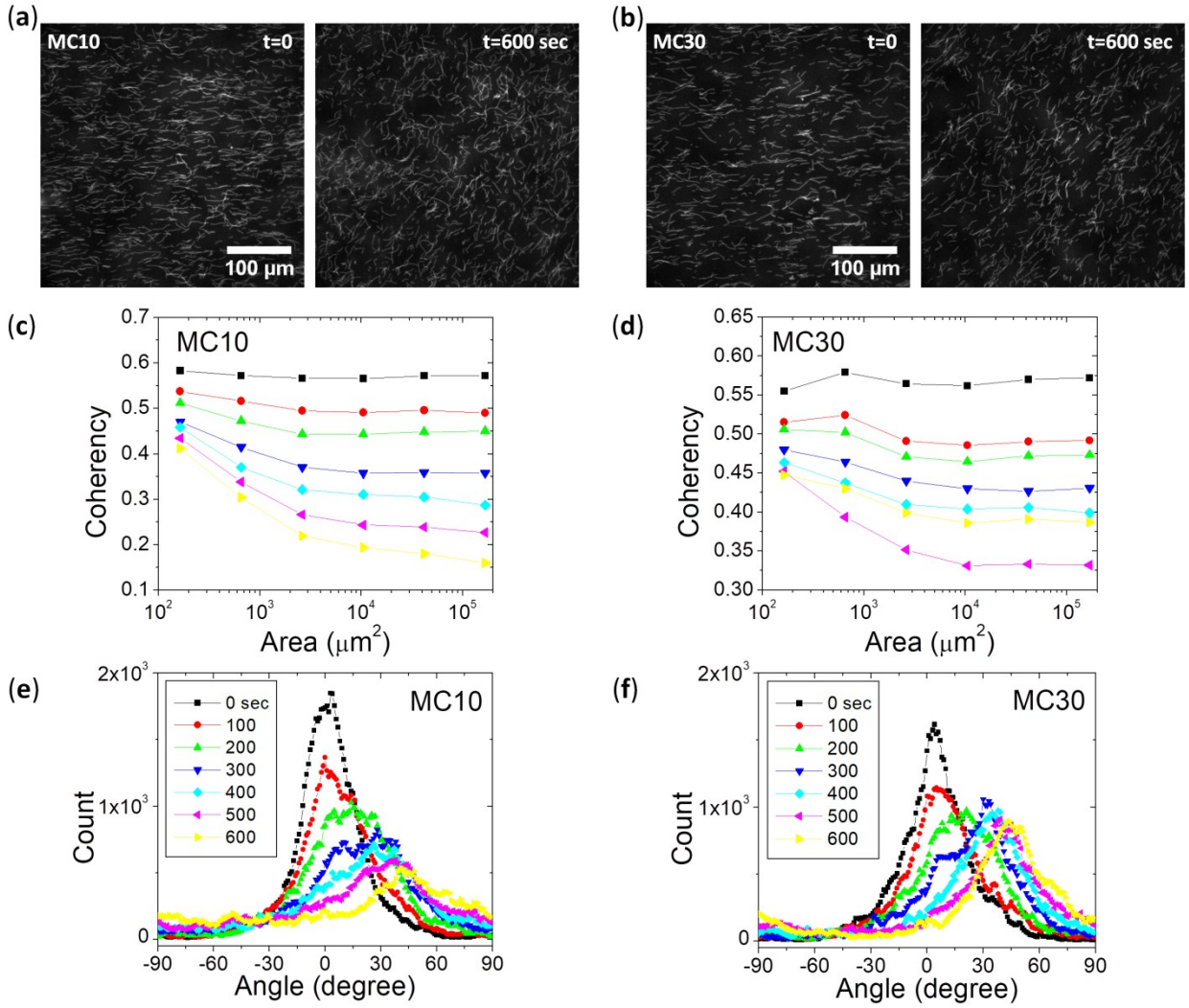

Supplementary Fig. 4: Coherency of MT orientation and local orientation histogram in the active layer formed in the presence of MC at two different concentrations, MC10 **(a, c, e)** and MC30 **(b, d, f)**. (a, b): time-lapsed fluorescence images (two different time frames, 0 and 600 sec) showing diluted visible MTs in the active layers. Scale bars: 100 μm. (c, d): Coherency plotted as a function of ROI size on a log-scale. (e, f): histograms of the local orientations of MTs plotted with absolute count. The zero-degree angle means the orientation parallel to the horizontal axis on each image and the orientation rotates counterclockwise as the angle increases. **Discussion**: In general, the coherency increases with the MC concentration and decreases with time. At lower MC concentration, the coherency drops faster (compare the curves for MC10 with those of MC30). The two cases show the coherency generally that decreases rapidly with the ROI size at the small area regime and saturates as the area increases further. The saturation level is lower for the case of MC10.

Supplementary Figure 5

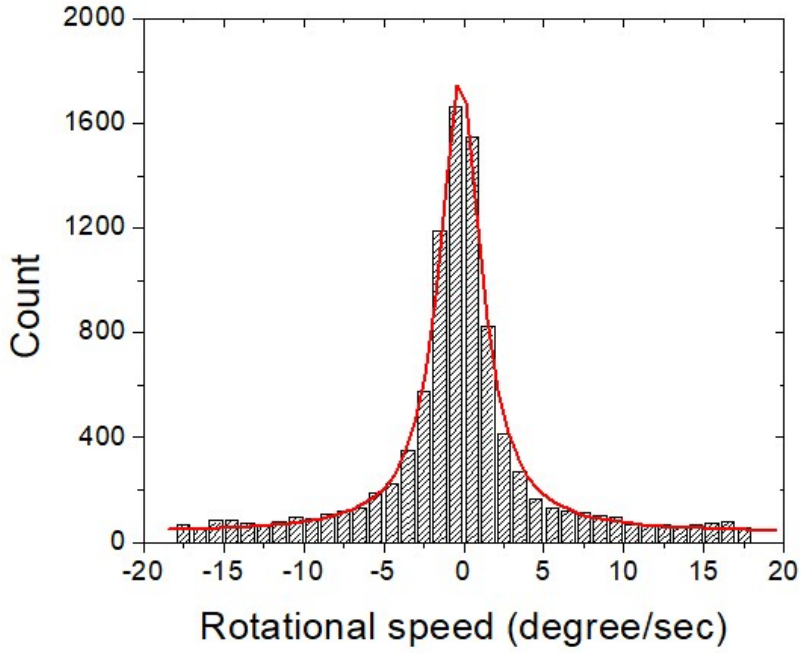

Supplementary Fig. 5: An example of the angular velocity (rotational speed) histogram and the Lorentzian curve fitting (red curve). The rotational speed is in degree/sec and this particular example shows the peak position (x_c) of −0.225 degree/sec.

Supplementary Figure 6

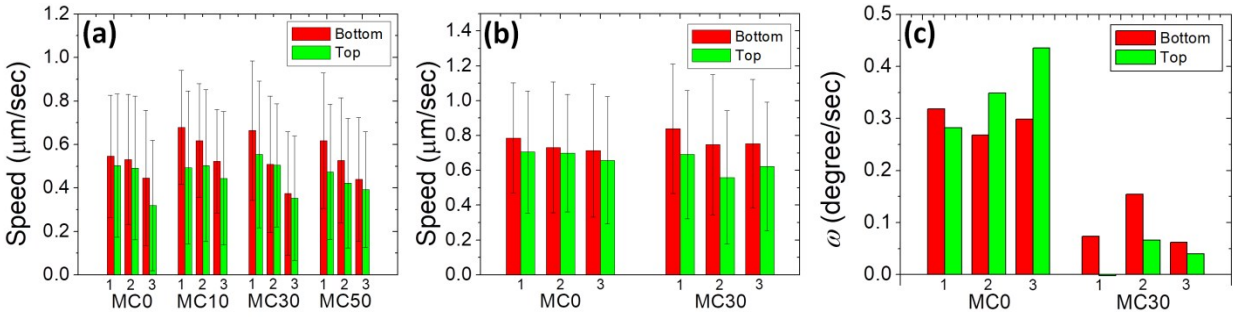

Supplementary Fig. 6: (a) MT gliding speed for four different MC concentrations. Red/green bars indicate results from bottom/top surface observation, respectively. The numbers, 1~3, for each set of the plot indicate the time sequence. Vertical lines are standard deviations. **(b-c)** MT gliding speed ((b)) and angular velocity ω ((c)) for two different MC concentrations. Red/green bars indicate results from bottom/top surface observation, respectively. The numbers, 1~3, for each set of the plot indicate three independent assays. Vertical lines in (b) are standard deviations. Here red bars in (c) are after multiplication of minus one, such that positive ω in this plot indicates counterclockwise rotation irrespective of the surface.

Supplementary Figure 7

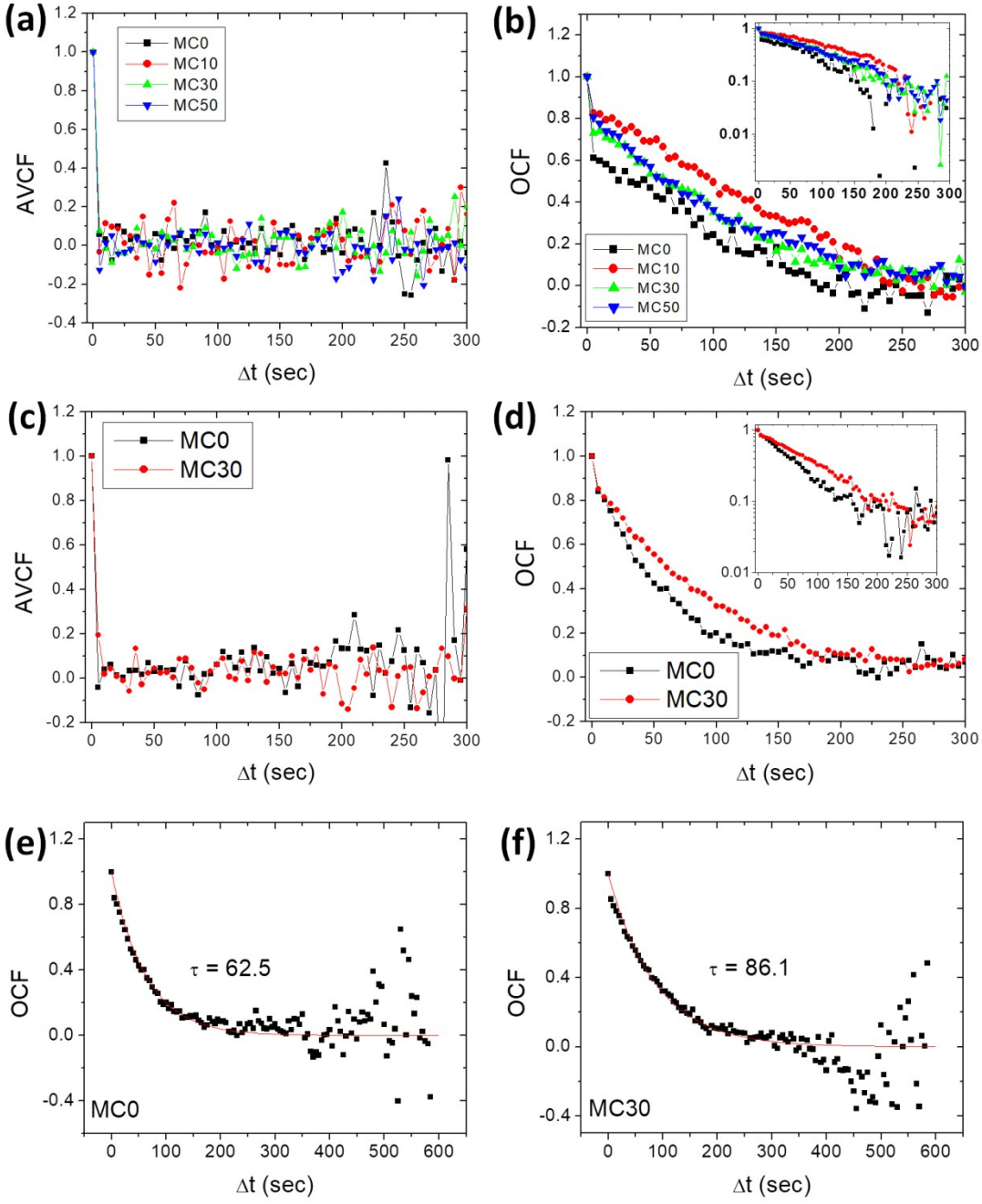

Supplementary Fig. 7: (a) Angular velocity correlation function (AVCF) and **(b)** orientation correlation function (OCF) as a function of lag time (Δt), obtained from the TOAST data tracing isolated gliding MTs. These plots show the assays analyzed for Fig. 4 (e, f) and Supplementary Fig. 6(a) for four different MC concentrations. The inset in panel (b) shows the OCFs plotted on a log-scale. AVCF drops immediately with Δt while OCF shows gradual decays with Δt. Data fluctuate more at higher Δt because the number of MTs traced decreases with increasing Δt. **(c)** Angular velocity correlation function (AVCF) and **(d)** orientation correlation function (OCF) as a

function of lag time (Δt), obtained from the TOAST data tracing isolated gliding MTs. These plots show the assays analyzed for Supplementary Fig. 6(b-c) for two different MC concentrations. The inset in panel (d) shows the OCFs plotted on a log-scale. **(e, f)** Exponentially decaying curves fitting (red lines) to the OCFs, using a single parameter exponential function, $y = e^{-t/\tau}$. τ in each panel indicates the relaxation time in sec.

Supplementary Figure 8 (caption next page)

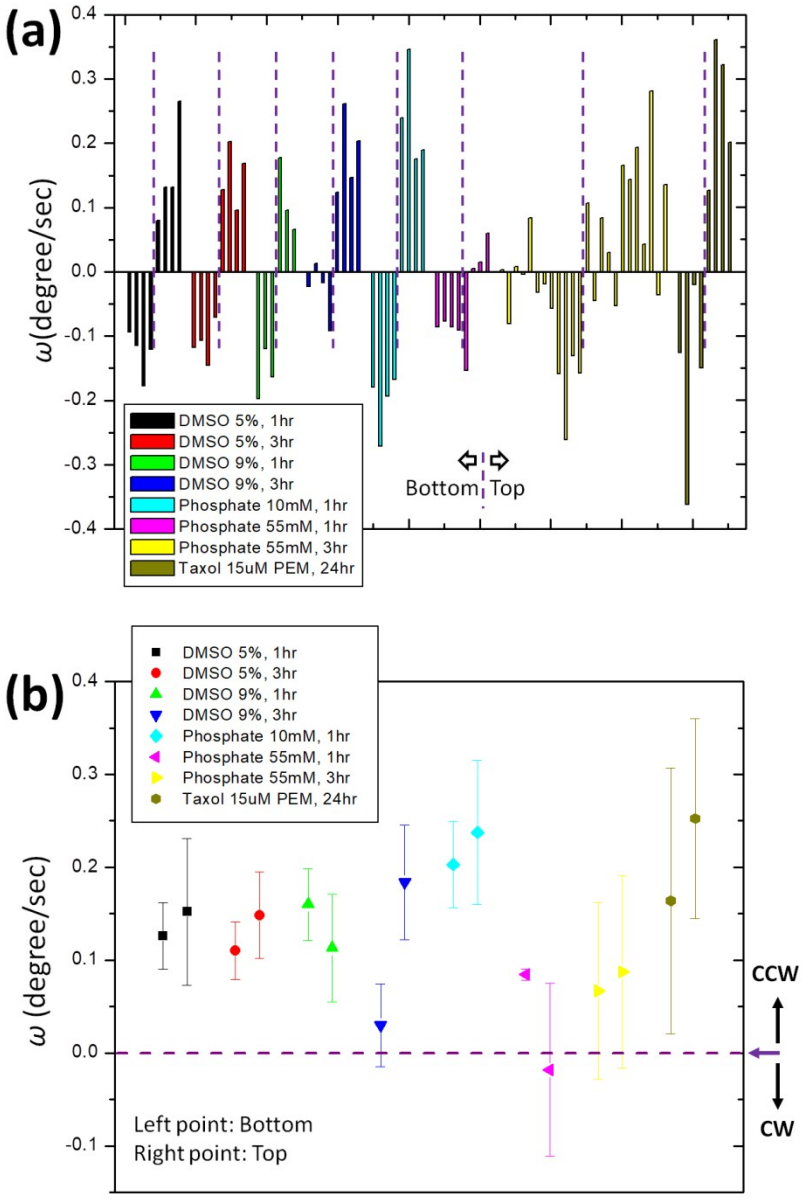

Supplementary Fig. 8: (a) Bar graph indicating mean angular velocities of MTs polymerized in various different conditions. At least two independent assays were performed for each case. Each bar is a result from an independent observation. Bars on the left side of vertical dotted lines (purple colored) are results from the bottom surface of the flow cell chamber, while bars on the right side are results from the top surface. These data show the measured values as it is. Therefore a negative value in the case of the bottom surface means counterclockwise rotation, while it indicates clockwise rotation for the case of the top surface. Preference of the counterclockwise rotation is apparent on both surfaces. For the cases of DMSO, the legend indicates DMSO concentration in %

(in PEM buffer) and incubation time. Tubulin concentration during polymerization was 2.5 mg/ml. For the cases of Phosphate, the legend indicates phosphate concentration and incubation time. Tubulin concentration during polymerization was 2.5 mg/ml. Note that 2 μM taxol was included in the phosphate buffer solutions. For the case of Taxol, PEM buffer including 15 μM taxol was used, the incubation time was 24 hr, and the tubulin concentration during polymerization was 0.5 mg/ml. All the buffer solutions included 1 mM GTP and 4 ~ 6 mM $MgCl_2$. **(b)** Averages with standard deviations (vertical lines) of the data in (a) taken for each case (color coded). The left/right data point in each set means the average for the case of bottom/top surface. Data from the bottom surface was multiplied by -1. As a result, a positive value in this graph indicates counterclockwise rotation irrespective of the surface.

Supplementary Figure 9

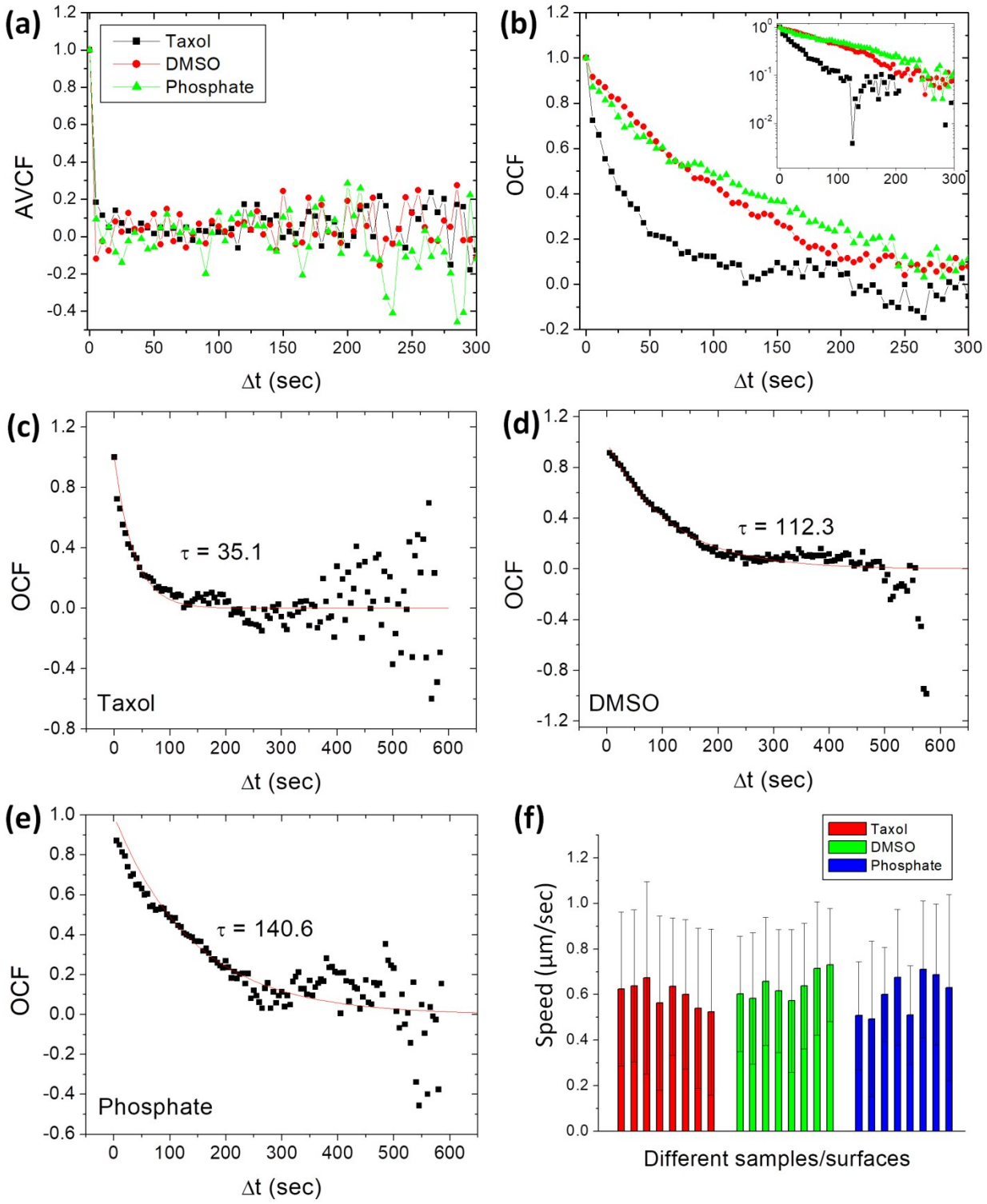

Supplementary Fig. 9: Three cases among all the conditions in Supplementary Fig. 8 were taken for the correlation analysis. These three conditions are (1) PEM buffer with 15 μM taxol (Taxol), (2) PEM with 5 % DMSO, 1hr polymerization (DMSO) and (3) 55 mM Phosphate buffer with 2 μM taxol, 1 hr polymerization (Phosphate). **(a)** Angular velocity correlation function (AVCF) as a function of lag time (Δt). **(b)** Orientation correlation function (OCF) as a function of Δt. (Inset: the same plot on a log-scale). **(c-e)** Exponentially decaying curves fitting (red lines) to the OCFs in (b), using a single parameter exponential function, $y = e^{-t/\tau}$. τ in each panel indicates the relaxation time in sec. **(f)** Mean MT gliding speeds for the three selected tubulin polymerization conditions. Each bar is a result from an independent observation (see Supplementary Fig. 8a).

Supplementary Figure 10

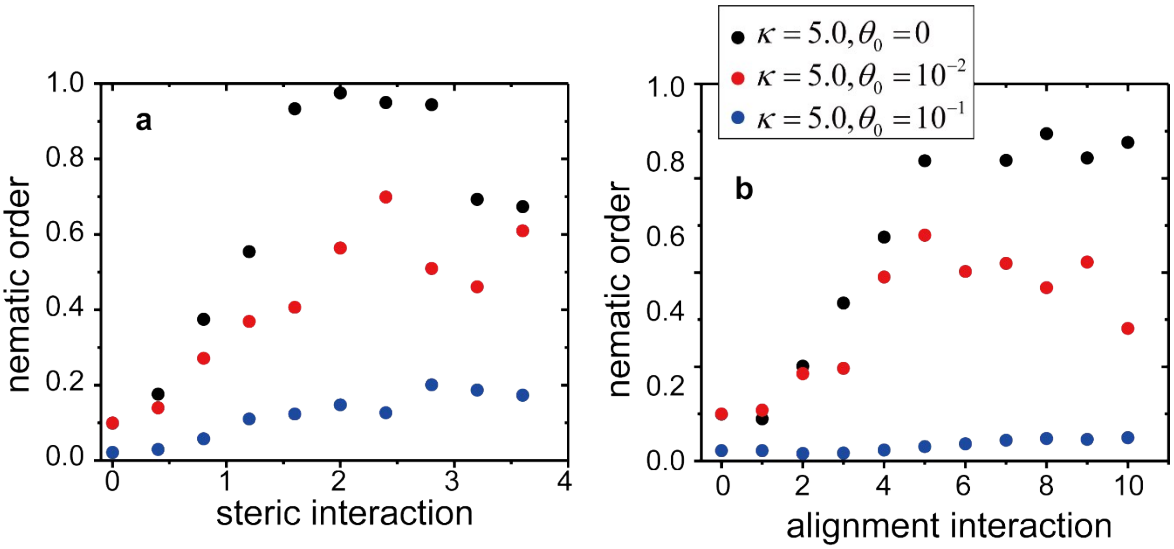

Supplementary Fig. 10: The nematic order parameter for $N = 256$ filaments of $M = 32$ monomers each, density $\rho = 0.44$, bending rigidity $\kappa = 5$ and various spontaneous curvatures θ_0 with steric interactions, β (a), and with alignment interactions, α (b), respectively.